

Article

Bias Effects on g- and s-Factors in Westcott Convention

Hideo Harada 

Nuclear Human Resource Development Center, Japan Atomic Energy Agency, Tokai-mura, Ibaraki 319-1195, Japan; harada.hideo@jaea.go.jp

Featured Application: This paper provides a size of bias on g- and s-factors in Westcott convention, induced by a joining function shape, neutron temperature, and sample temperature, for both 1/v isotopes and non-1/v isotopes. Its impact on neutron activation reaction rate is also discussed. Quantitative results are used for accuracy improvement of neutron activation analysis and neutron capture cross sections.

Abstract: For accuracy improvement of neutron activation analysis and neutron capture cross sections, bias effects are investigated on g- and s-factors in the Westcott convention. As origins of biases, a joining function shape, neutron temperature, and sample temperature have been investigated. Biases are quantitatively deduced for two 1/v isotopes (^{197}Au , ^{59}Co) and six non-1/v isotopes (^{241}Am , ^{151}Eu , ^{103}Rh , ^{115}In , ^{177}Hf , ^{226}Ra). The s-factor calculated with a joining function deduced recently by a detailed Monte Carlo simulation is compared to s-factors calculated with traditional joining functions by Westcott. The results show the bias induced by the sample temperature is small, in the order of 0.1% for the g-factor and in the order of 1% for the s-factor. On the other hand, the bias size induced by a joining function shape for the s-factor depends significantly on both isotopes and neutron temperature. As a result, the reaction rates are also affected significantly. The bias size for the reaction rate is given in the case of an epithermal neutron index $r = 0.1$, for the eight isotopes.



Citation: Harada, H. Bias Effects on g- and s-Factors in Westcott Convention. *Appl. Sci.* **2021**, *11*, 6558. <https://doi.org/10.3390/app11146558>

Academic Editor: Marco Di Luzio

Received: 31 May 2021
Accepted: 13 July 2021
Published: 16 July 2021

Publisher's Note: MDPI stays neutral with regard to jurisdictional claims in published maps and institutional affiliations.



Copyright: © 2021 by the author. Licensee MDPI, Basel, Switzerland. This article is an open access article distributed under the terms and conditions of the Creative Commons Attribution (CC BY) license (<https://creativecommons.org/licenses/by/4.0/>).

Keywords: neutron activation analysis; neutron capture cross section; bias effect; neutron resonance; joining function; Westcott convention; Doppler broadening; sample temperature; neutron temperature

1. Introduction

Neutron activation analysis (NAA) using well-thermalized neutrons is a powerful tool utilized in various application fields. For NAA, information of neutron capture cross sections for isotopes to be analyzed and a neutron energy spectrum at an irradiation position are required. The energy spectrum of well-thermalized neutrons is approximated to be the sum of two components, a Maxwellian distribution corresponding to neutron temperature T_n and an epithermal dE/E flux distribution cut off at a suitable lower limit of energy. This flux notation is known as the Westcott convention [1] and is widely utilized in NAA. The neutron activation reaction rate R_x for the isotope x is expressed as

$$R_x = N_x \cdot \phi_0 \cdot \sigma_{x0} \cdot (g_x + r \cdot s_x) \quad (1)$$

where N_x is the number of the isotope x , ϕ_0 is the neutron flux, r is the epithermal index that represents the relative strength of the epithermal component, σ_{x0} is the cross section at 0.0253 eV neutrons, and the g- and s-factors are functions of T_n . The g- and s-factors depend on the departure of the cross-section law from the 1/v form (for a 1/v law, $g = 1$ and $s = 0$).

NAA is also one of the powerful tools determining neutron capture cross sections [2–5]. In order to improve the accuracy of NAA and/or neutron capture cross sections, a number of improvements have been made. The epithermal dE/E flux distribution was refined as $dE/E^{1+\alpha}$ [6], introducing an adjusting parameter α , and the s-factor was revised to

reflect the refined form. Recently, finer forms have been proposed by introducing two [7] or three [8] adjusting parameters and were used for accuracy improvement of resonance integrals and s-factor [7].

The cut-off region of the epithermal dE/E flux component is often approximated by a unit step function, which was introduced in Westcott's report in 1959 [1]. In the revised version of Westcott's report in 1970 [9], several revised forms of Δ_i^W ($i = 1$ to 4), called now joining functions, were introduced. The joining function expresses not only a sharp cut-off energy of the dE/E flux component but also a rather more gradual cut and an additional bump. The systematic effect on the s-factor induced by a change in a joining function from a unit step function was studied for re-evaluation of neutron capture cross section of ^{241}Am measured by a neutron activation method [10]. Neutron activation analysis for isotopes with a prominent neutron resonance below 0.5 eV as in ^{241}Am needs a careful analysis taking into account the resonance below 0.5 eV; an experimental technique has been developed to eliminate or reduce the low-energy resonance effect [5].

In the study of resonance integrals or s-factor in [7], adjusting parameters in the joining function Δ_4^W was investigated from the neutron energy spectrum obtained by a detailed Monte Carlo simulation. It is expressed as Δ_4^H in this paper, and its formula is given in Section 2. Although a height of a bump in both forms is almost the same, there is a noticeable difference on a high-energy side tail of the bump up to a few eV. Therefore, in the case of the Δ_4^H form, a bias effect on s-factor and reaction rate might be non-negligible for isotopes if there are huge resonances below a few eV. This paper studies in detail the bias on the s-factor and the reaction rate induced by the joining function form Δ_4^H .

As the other bias origins on g- and s-factors, neutron temperature dependence has already been studied in the report by Westcott [9]. Recently, the neutron temperature effect has been investigated by taking into account Westcott's Δ_i^W functions [11]. An experimental technique to measure neutron temperature was developed because of its importance [12]. Here, it should be noted that neutron temperature characterizing a Maxwell distribution at sample position is not the same as sample temperature, since neutron absorption reactions distort the neutron energy distribution, and the leakage rate of neutrons through a sample guide hole depends on neutron energy. Therefore, sample temperature should be distinguished from neutron temperature.

Sample temperature affects the shape of a resonance peak, since it is broadened due to Doppler effect. A bias effect by sample temperature might be noticeable for isotopes with resonances around the cut-off energy of the joining function. However, the sample temperature effect has not been quantitatively reported, so far.

In this study, bias effects on Westcott g- and s-factors are investigated. The s-factor calculated by using the joining function based on a full Monte Carlo simulation is compared with those using traditional joining functions in Westcott's report. The g- and s-factors are calculated for sample temperatures 300 K and 1000 K, for neutron temperatures ranging from 20 K to 1600 K, and for two $1/v$ isotopes (^{197}Au , ^{59}Co) and six non- $1/v$ isotopes (^{241}Am , ^{151}Eu , ^{103}Rh , ^{115}In , ^{177}Hf , ^{226}Ra). The bias size for the reaction rate is also evaluated in the case of an epithermal neutron index $r = 0.1$, for these eight isotopes. The formula and calculation methods in this paper can be utilized for any isotope. Although neutron self-absorption correction is known to be an important bias [13], this correction is outside the scope of this work.

2. Formulas and Calculation Methods

The formulas used in this paper are described in this section, together with practical calculation methods.

A neutron energy spectrum for thermalized reactor neutrons by Westcott et al. [9], where the spectrum is approximated by the sum of Maxwellian and $1/E$ distributions, is expressed as

$$\phi(E) = \phi_{th}(E) + \phi_{epi}(E) = \phi_{th} \cdot \frac{2}{\sqrt{\pi}} \cdot \sqrt{\frac{T_n}{T_0}} \cdot \frac{E}{(kT_n)^2} \cdot e^{-E/kT_n} + \phi_{epi} \cdot \frac{\Delta(E)}{E} \quad (2)$$

where E is the neutron energy, T_n the temperature of neutrons defined in the Maxwellian distribution, k the Boltzmann constant, and $\Delta(E)$ a joining function. The parameters ϕ_{th} and ϕ_{epi} are constants expressing the intensities of thermal and epithermal neutron flux components. As a joining function, several types have been proposed such as $\Delta_2^W(E)$ and $\Delta_4^W(E)$, as shown in Westcott's reports [9]. Δ_4^W has been recognized as the most appropriate function among various functions reported by Westcott et al. However, the simple Δ_2^W shape or, even more, a sharp cut-off function expressed by a unit step function has been utilized in both NAA and neutron capture cross section measurements, since a bias for reaction rate originating in the joining function is thought to be negligible for ideal $1/v$ isotopes. Δ_4^H is the joining function adjusted to reproduce a neutron energy spectrum at an irradiation position of a research reactor by using a Monte Carlo simulation with detailed configuration [7]. The formulas of $\Delta_2^W(E)$, $\Delta_4^W(E)$, and Δ_4^H are given below:

$$\Delta_2^W(E) = \frac{1}{1 + \left(\frac{4.95kT_n}{E}\right)^7} \quad (3)$$

$$\Delta_4^W(E) = \frac{1}{1 - \frac{0.26}{1 + \left(\frac{E}{16.4kT}\right)^5} + \left(\frac{4.75kT_n}{E}\right)^7} \quad (4)$$

$$\Delta_4^H(E) = \frac{1}{1 - \frac{0.26}{1 + \left(\frac{E}{26.1kT_n}\right)^{1.93}} + \left(\frac{5.06kT_n}{E}\right)^{5.88}} \quad (5)$$

the joining functions Δ_2^W , Δ_4^W , Δ_4^H for neutron temperature $T_n = 300$ K are plotted in Figure 1a by solid, dotted, and dashed line, respectively. There are bumps at around 0.23 and 0.27 eV for Δ_4^W and Δ_4^H , respectively. The cut-off energy for both Δ_2^W and Δ_4^H is about 0.13 eV, which is a little higher than 0.12 eV for Δ_4^W . The difference of a high-energy side tail of the bump should be noted; there exists a larger component in Δ_4^H compared to Δ_4^W in a neutron energy region from about 0.5 eV to a few eV. The same for neutron temperature 1000 K are plotted in Figure 1b. The cut-off energy and bump peak energy are shifted by a factor 1000/300. It is anticipated that the reaction rates for isotopes with a resonance at around the cut-off energy or bump peak energy will be affected significantly by using different joining functions.

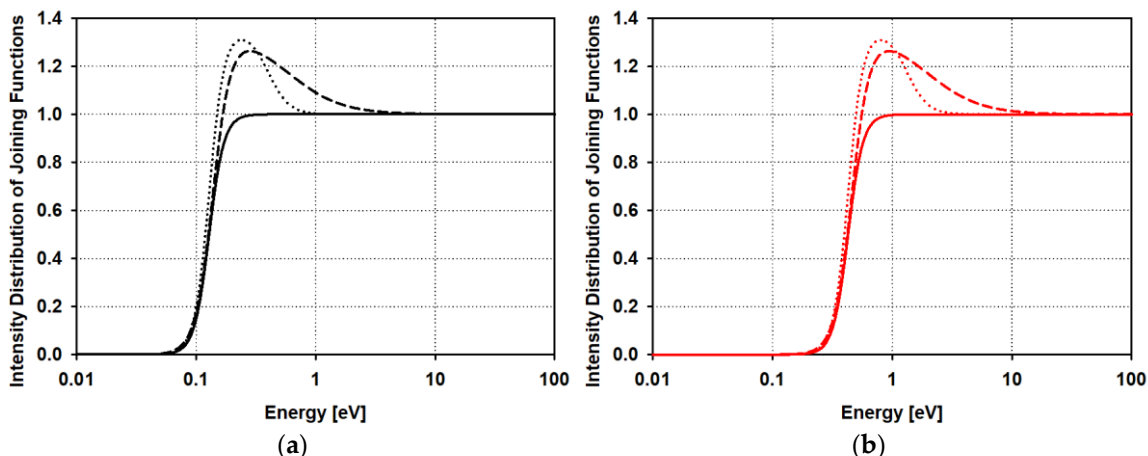


Figure 1. Joining functions Δ_2^W (solid line), Δ_4^W (dotted line), Δ_4^H (dashed line) for neutron temperatures (a) $T_n = 300$ K; (b) $T_n = 1000$ K.

The g factor in Equation (1), defined as the ratio of pure Maxwellian flux-weighted cross section ($\hat{\sigma}_m$) to the cross section at 0.0253 eV (σ_0), is expressed as

$$g(T_n, T_s) = \frac{\hat{\sigma}_m}{\sigma_0} = \frac{1}{\sigma_0} \frac{2}{\sqrt{\pi}} \sqrt{\frac{T_n}{T_0}} \int_0^\infty \frac{E}{(kT_n)^2} \cdot e^{-\frac{E}{kT_n}} \cdot \sigma(E, T_s) dE \quad (6)$$

where sample temperatures (T_s) are explicitly indicated in the cross section $\sigma(E, T_s)$.

The s factor in Equation (1), representing the ratio of resonance integral after subtraction of the 1/v component to σ_0 , is expressed as

$$s(T_n, T_s) = \frac{1}{\sigma_0} \frac{2}{\sqrt{\pi}} \sqrt{\frac{T_n}{T_0}} \int_0^\infty \left(\sigma(E, T_s) - g(T_n, T_s) \cdot \sigma_0 \cdot \sqrt{\frac{kT_0}{E}} \right) \cdot \frac{\Delta(E)}{E} dE \quad (7)$$

Hereafter, the s-factor calculated using the joining functions $\Delta_2^W, \Delta_4^W, \Delta_4^H$ as $\Delta(E)$ in Equation (7) are expressed as s_2^W, s_4^W, s_4^H .

Fine-mesh numerical data of the cross section are available in a website of nuclear data center [14] for $T_s = 0$ and 300 K, corresponding to JENDL-4.0 nuclear data library [15]. The Doppler-broadened cross section at any sample temperature can be deduced from the unbroadened cross section $\sigma(E, 0)$ at $T_s = 0$ K. The Doppler-broadened cross section for T_s is expressed by the next equation based on a free-gas model [16]:

$$\sigma(E, T_s) = \frac{1}{W_D \sqrt{\pi}} \int_0^\infty \left(e^{-\frac{4(E-\sqrt{E \cdot E'})^2}{W_D^2}} - e^{-\frac{4(E+\sqrt{E \cdot E'})^2}{W_D^2}} \right) \sigma(E', 0) \sqrt{\frac{E'}{E}} dE' \quad (8)$$

the Doppler width W_D in Equation (8) is given by

$$W_D(E, T_s) = \sqrt{\frac{4 \cdot E \cdot kT_s}{A}} \quad (9)$$

where A is the ratio of the sample mass to the neutron mass.

The capture cross sections of ^{241}Am deduced using Equation (8) for $T_s = 300$ and 1000 K are shown by a black solid line and a red solid line in Figure 2a, and those of ^{151}Eu in Figure 2b. The number of mesh points used for integration of Equation (8) is about 65 k for ^{241}Am and 22 k for ^{151}Eu .

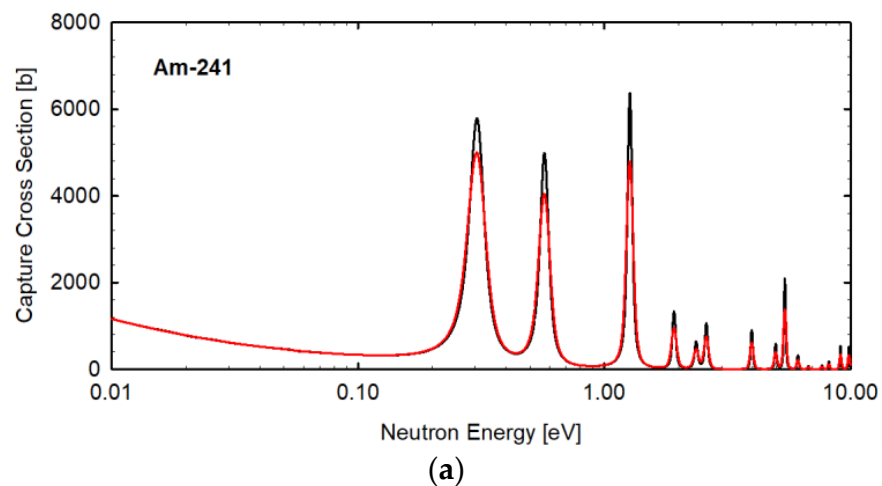


Figure 2. Cont.

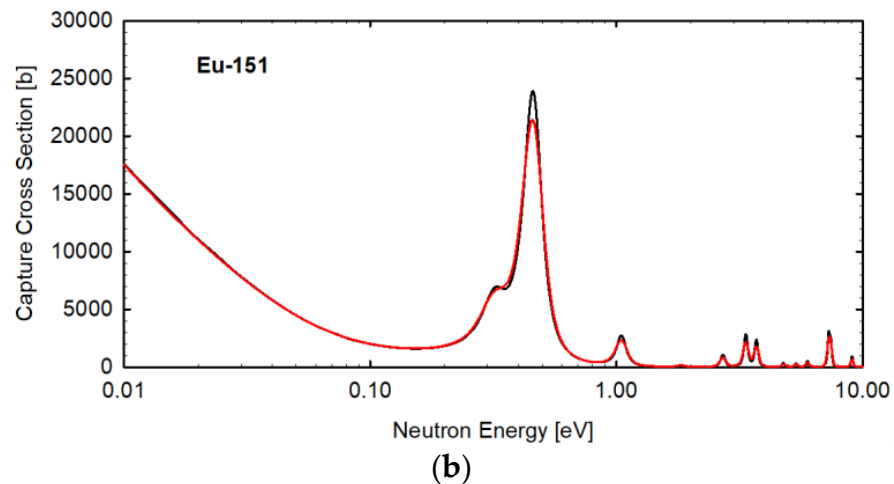


Figure 2. (a) Capture cross section of ^{241}Am for sample temperatures $T_s = 300\text{ K}$ (black solid line) and $T_s = 1000\text{ K}$ (red solid line) calculated with a free-gas model and JENDL-4.0 data at $T_s = 0\text{ K}$; (b) the same with (a) for ^{151}Eu .

3. Results and Discussions

The sample temperature effect on the g - and s -factors is discussed based on calculations for the non $1/v$ isotopes ^{241}Am and ^{151}Eu , in which this effect is expected to be shown more clearly than in other isotopes, since they have prominent resonances near about 0.31 eV and 0.46 eV, respectively. Next, a joining function shape effect as a function of neutron temperature is discussed for eight isotopes, ^{241}Am , ^{151}Eu , ^{197}Au , ^{59}Co , ^{103}Rh , ^{115}In , ^{177}Hf , and ^{226}Ra . The sample temperature is fixed at $T_s = 300\text{ K}$ in the discussion of a joining function shape effect. ^{197}Au and ^{59}Co are well known as $1/v$ isotopes and used for neutron flux determination as monitor samples. ^{103}Rh , ^{115}In , ^{177}Hf , and ^{226}Ra are non $1/v$ isotopes and have prominent resonances between 0.5 eV and 1.5 eV. The capture cross sections of ^{197}Au , ^{59}Co , ^{103}Rh , ^{115}In , ^{177}Hf , and ^{226}Ra obtained from JENDL-4.0 at $T_s = 300\text{ K}$ [14] are shown in Figure 3a–f and used in the calculations. At last, biases originated in a joining function shape for the s -factor and the reaction rate are discussed using the calculation results obtained for all eight isotopes.

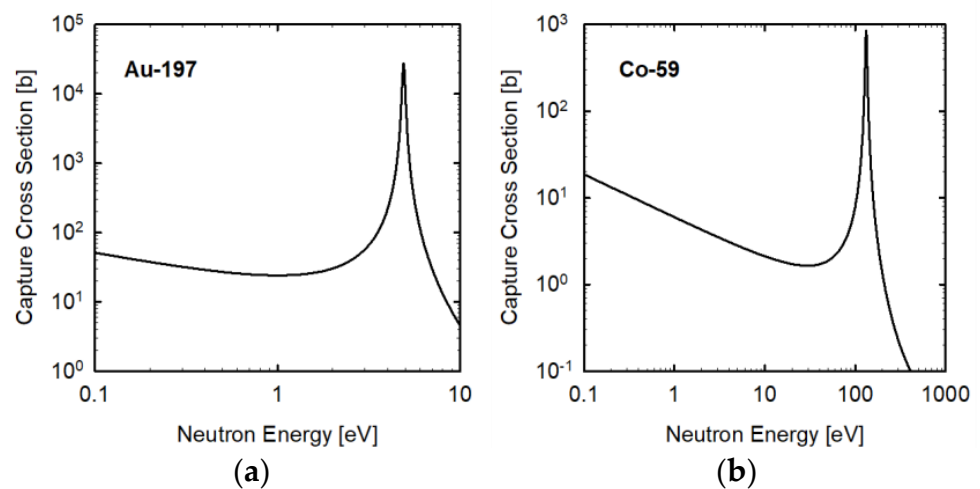


Figure 3. Cont.

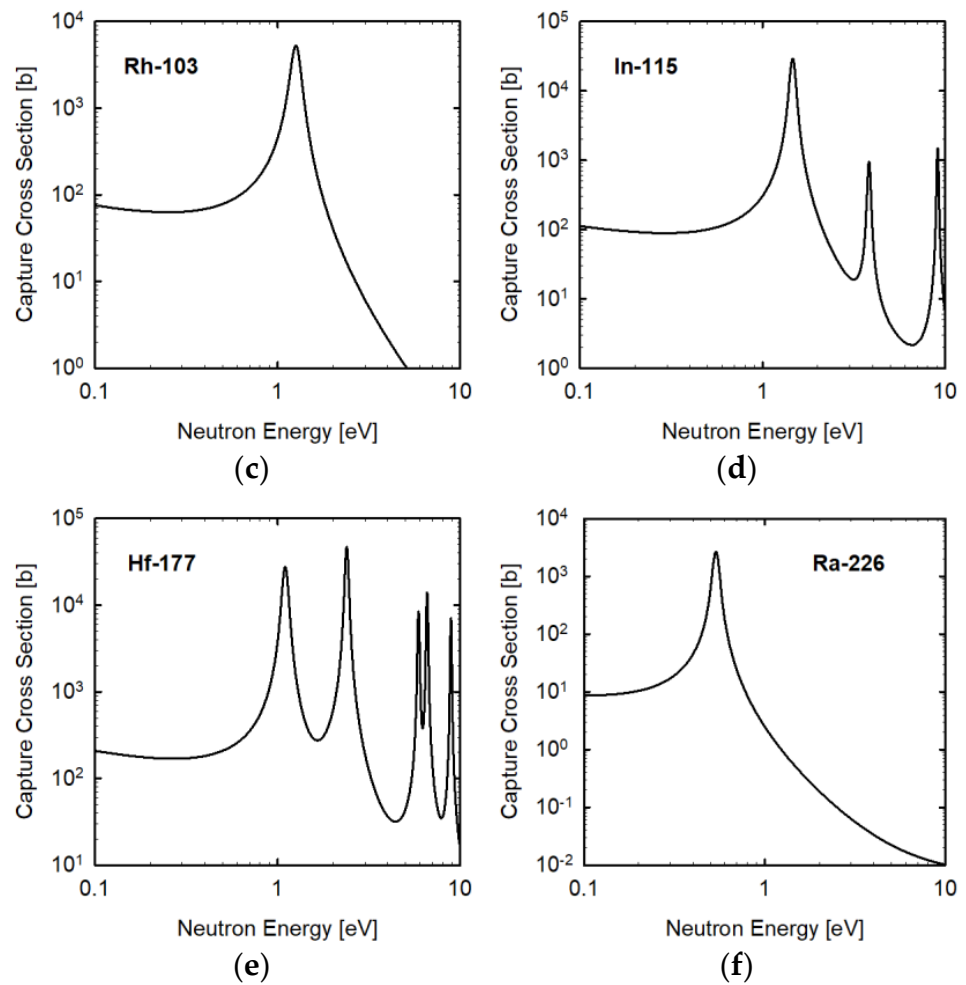


Figure 3. (a) Capture cross sections for $T_s = 300$ K of ^{197}Au ; (b) ^{59}Co ; (c) ^{103}Rh ; (d) ^{115}In ; (e) ^{177}Hf ; (f) ^{226}Ra .

3.1. g -Factors for ^{241}Am and ^{151}Eu for Sample Temperatures of 300 and 1000 K

The g -factor for ^{241}Am is calculated by inserting $\sigma(E, T_s)$ into Equation (6) as a function of neutron temperature T_n , for two sample temperatures, i.e., $T_s = 300$ K (black) and 1000 K (red), and plotted in Figure 4a. Two curves are almost degenerated. The g -factor is almost equal to the unity in the neutron energy region below 400 K and gradually increases as the neutron temperature rises, since the first neutron resonance at 0.31 eV starts to contribute to this increase. Figure 4b is an expanded version of Figure 4a, showing the neutron energy region between 250 and 450 K. In this neutron temperature range, the deviation of the g -factor from unity is from 1% to 9%. If neutron temperature is determined with an uncertainty of 25 K, the g -factor can be estimated with an uncertainty of about 1% using the data shown in this figure.

Figure 4c shows the ratio of g -factor at $T_s = 1000$ K to that at 300 K for ^{241}Am . Figure 4d is the expanded version of Figure 4c. The maximum deviation from the unity is about 0.5% at a neutron temperature near 600 K. It is only 0.3% for a limited region from 250 K to 450 K, as shown in Figure 4d. Therefore, for most applications not requiring accuracy below 1%, the sample temperature effect on the g -factor can be neglected. It should be remembered that this effect needs to be considered for special applications such as neutron standard cross section studies aiming at accuracy in the order of 0.1%.

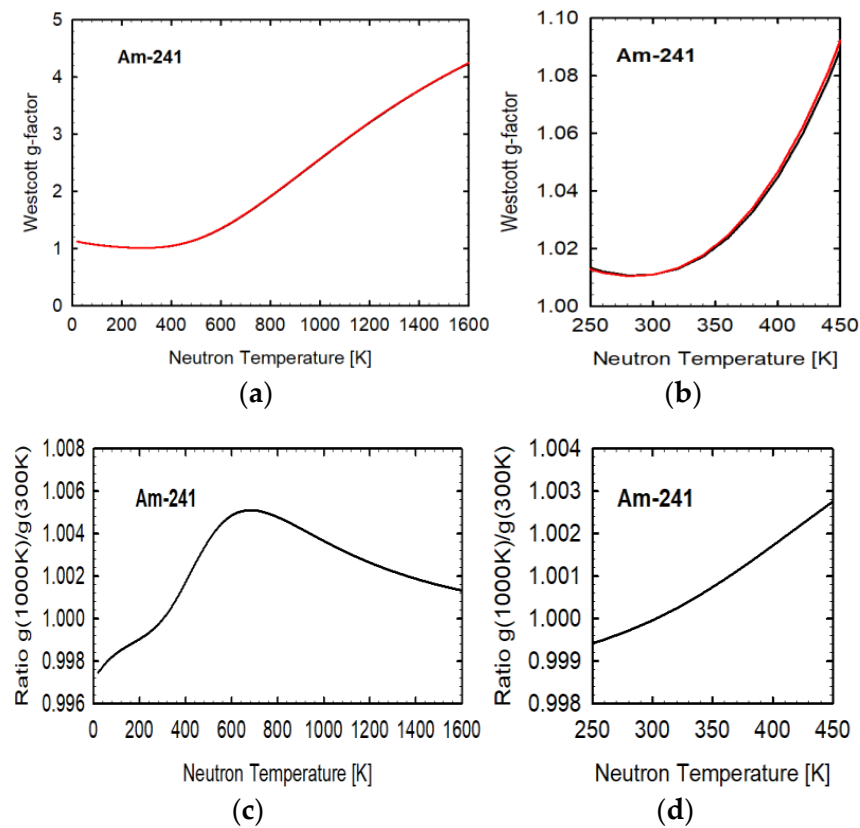


Figure 4. (a) Westcott g-factor for ^{241}Am as a function of neutron temperature T_n , for two sample temperatures, $T_s = 300\text{ K}$ (black) and 1000 K (red); (b) Expanded figure of (a); (c) Ratio of Westcott g-factor for $T_s = 1000\text{ K}$ to that for 300 K ; (d) Expanded figure of (c).

Figure 5 shows the g-factor calculated for ^{151}Eu . The change of the g-factor as a function of neutron temperature for ^{151}Eu is more moderate compared to the case of ^{241}Am , as shown in Figure 5a. This tendency can be explained by the fact that the first prominent resonance energy of ^{151}Eu is about 1.5 times higher than that of ^{241}Am . By comparing the g-factors of ^{241}Am and ^{151}Eu in a limited region from 250 K to 450 K, it is noticed that the difference of the slopes is significant, and the ratio of these g-factors is sensitive to neutron temperature. Although the effectiveness using a Zr–Au–Lu alloy is known to determine neutron temperature [12], the combinational use of these isotopes would provide additional and independent information on neutron temperature. The sample temperature effect for ^{151}Eu shown in Figure 5c,d is in the same order of that for ^{241}Am , as discussed above.

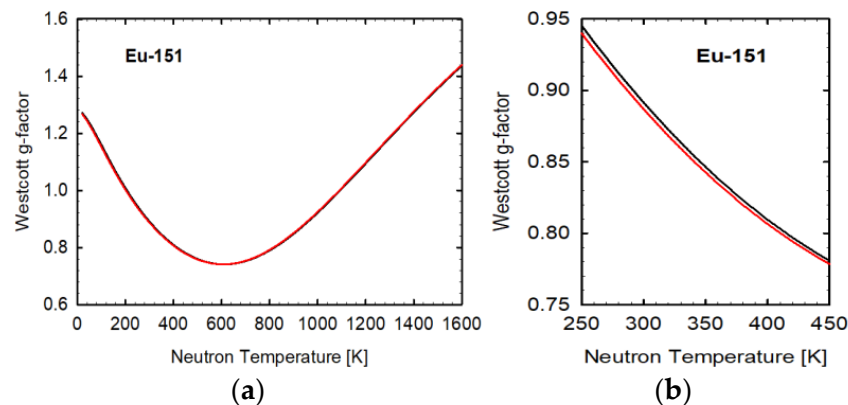


Figure 5. Cont.

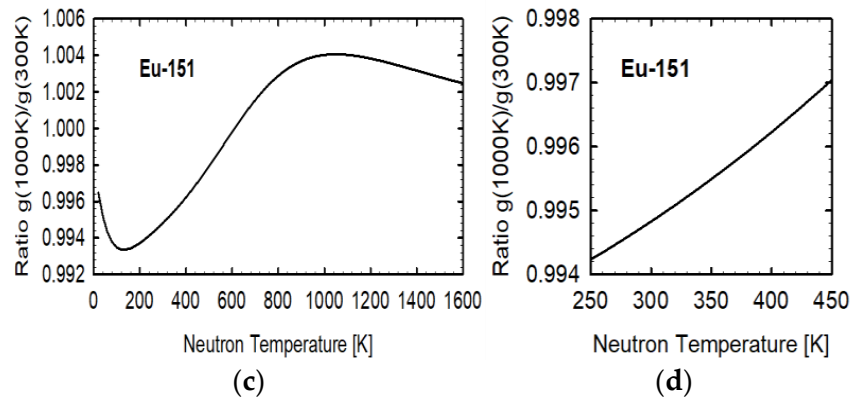


Figure 5. (a) Westcott g-factor for ^{151}Eu as a function of neutron temperature T_n , for two sample temperatures, $T_s = 300\text{ K}$ (black) and 1000 K (red); (b) Expanded figure of (a); (c) Ratio of Westcott g-factor for $T_s = 1000\text{ K}$ to that for 300 K ; (d) Expanded figure of (c).

3.2. s-Factors for ^{241}Am and ^{151}Eu for Sample Temperatures of 300 and 1000 K

The s-factors for ^{241}Am are plotted in Figure 6a as a function of neutron temperature T_n , for two sample temperatures, $T_s = 300\text{ K}$ (black) and 1000 K (red), which are calculated by inserting $\sigma(E, T_s)$ into Equation (7). The s-factors corresponding to $\Delta_2^W(E)$, $\Delta_4^W(E)$, and $\Delta_4^H(E)$, that is, s_2^W , s_4^W , s_4^H , are shown by solid-, dotted-, and dashed lines, respectively. The difference for two sample temperatures is so small that black and red lines are not separated in Figure 6a. To show the difference between two sample temperatures, the ratios of s-factors are plotted in Figure 6c,d for three kinds of joining functions, indicated by solid-, dotted-, and dashed lines, respectively. The deviation of the ratio from the unity is less than 0.5% for a wide neutron temperature range from 0 K to 1000 K.

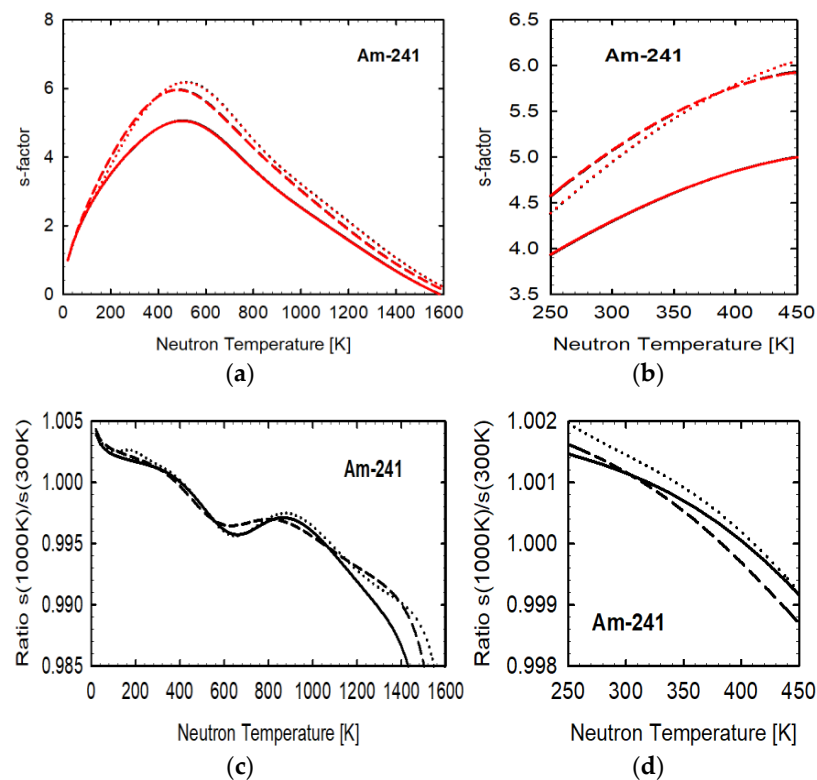


Figure 6. Cont.

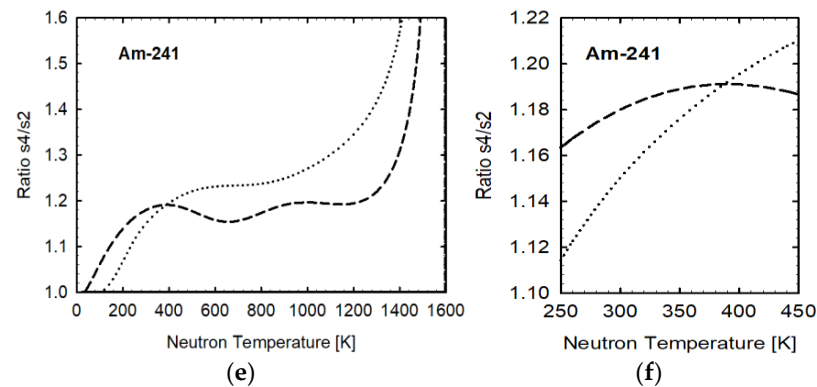


Figure 6. (a) s -factors, s_2^W (solid line), s_4^W (dotted line), s_4^H (dashed line) for ^{241}Am as a function of neutron temperature T_n , for sample temperatures $T_s = 300$ K (black) and 1000 K (red); (b) Expanded figure of (a); (c) Ratios of s_2^W (solid line), s_4^W (dotted line), s_4^H (dashed line) between $T_s = 300$ K and 1000 K; (d) Expanded figure of (c); (e) Ratios of s -factors, s_4^W/s_2^W (dotted line) and s_4^H/s_2^W (dashed line) for $T_s = 300$ K; (f) Expanded figure of (e).

Contrary to the sample temperature effect, there are noticeable differences between s -factors corresponding to $\Delta_2^W(E)$, $\Delta_4^W(E)$, and $\Delta_4^H(E)$, as shown in Figure 6a,b. Figure 6e,f shows the ratio of s -factors calculated with $\Delta_4^W(E)$ or $\Delta_4^H(E)$ to that calculated with $\Delta_2^W(E)$. The deviation of the ratio from the unity is as large as about 20% for a wide neutron temperature range. In Figure 6b, the expanded version of Figure 6a, the difference between s_4^W and s_2^W , and also between s_4^H and s_2^W , is clearly shown. A difference of a few % points is also noticed for the ratios between s_4^W/s_2^W and s_4^H/s_2^W in Figure 6e,f.

The s -factors for ^{151}Eu are plotted in Figure 7a–f, as in Figure 6 for ^{241}Am . As shown in Figure 7a, the s -factor for ^{151}Eu crosses the zero at about 160 K and 1160 K. To show the difference quantitatively between two sample temperatures, the ratios of s -factors are plotted in Figure 7c,d for three kinds of joining functions, indicated by solid-, dotted-, and dashed lines, respectively. The deviation of the ratio from the unity is about 0.5 to 1.5% in the neutron temperature range from 300 K to 400 K. However, for example, in the case of an epithermal index $r = 0.1$, this sample temperature effect on a reaction rate is limited to the level in the order of 0.1%, since the absolute value of the s -factor for ^{151}Eu is small.

There is a noticeable difference between s -factors, s_4^W/s_2^W , and s_4^H/s_2^W , as shown in Figure 7e,f. The deviation of the ratio from the unity seems to diverge at about 160 K and 1160 K. The reason is that the value of the s -factor crosses the zero point at these neutron temperatures. Since the s -factor is close to zero at these points, the effect induced by the deviations on the reaction rate is limited. However, for the important neutron temperature region at about 300–400 K, the deviation from the unity is about 30% in the case of $\Delta_4^H(E)$ and strongly varies from 12% to 34% in the case of $\Delta_4^W(E)$. This observation demonstrates the importance of a careful determination of the joining function shape.

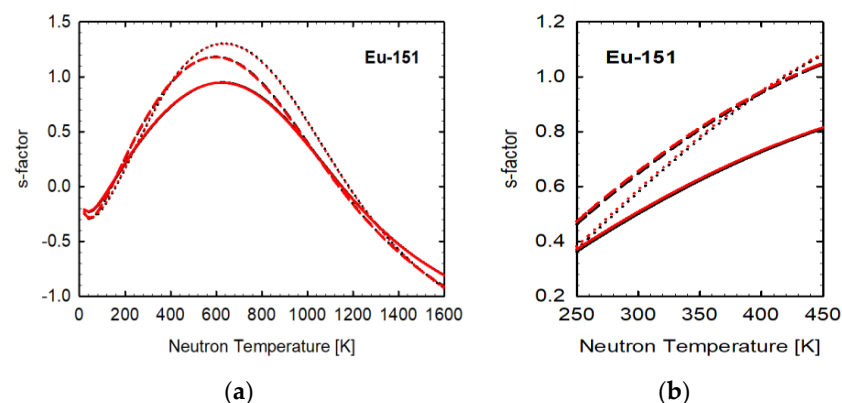


Figure 7. Cont.

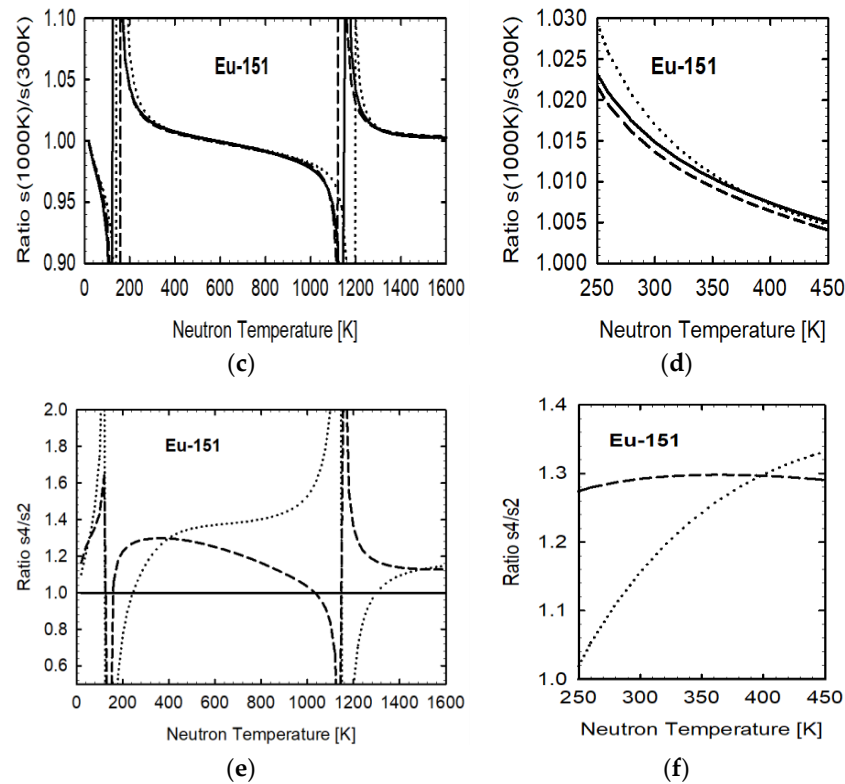


Figure 7. (a) s -factors, s_2^W (solid line), s_4^W (dotted line), s_4^H (dashed line) for ^{151}Eu as a function of neutron temperature T_n , for sample temperatures $T_s = 300$ K (black) and 1000 K (red); (b) Expanded figure of (a); (c) Ratios of s_2^W (solid line), s_4^W (dotted line), s_4^H (dashed line) between $T_s = 300$ K and 1000 K; (d) Expanded figure of (c); (e) Ratios of s -factors, s_4^W/s_2^W (dotted line) and s_4^H/s_2^W (dashed line) for $T_s = 300$ K; (f) Expanded figure of (e).

Hereafter, results are shown corresponding to the sample temperature of 300 K only, since its effect is small, as discussed for ^{241}Am and ^{151}Eu .

3.3. g - and s -Factors for ^{197}Au , ^{59}Co , ^{103}Rh , ^{115}In , ^{177}Hf , and ^{226}Ra

A joining function shape effect on g - and s -factor is discussed for other six isotopes, i.e., ^{197}Au , ^{59}Co , ^{103}Rh , ^{115}In , ^{177}Hf , and ^{226}Ra . The calculated g - and s -factors for these isotopes are plotted in Figures 8–13. Figures 8–13 (a) show g -factors, and (b) is the enlarged view of (a) in the neutron temperature region from 250 K to 450 K. Figures 8–13 (c) show s -factors, and (d) is the enlarged view of (c). Figures 8–13 (e) show the ratio of s -factors, that is, s_4^W/s_2^W and s_4^H/s_2^W , and (f) is the enlarged view of (e).

The capture cross section of ^{197}Au is used as the neutron cross section standard at 0.0253 eV, and the $1/v$ law can be applied well, as shown in Figure 3a. The deviation from the unity of the g -factor is only 0.6% at 0.0253 eV. The absolute value of the s -factor of ^{197}Au shown in Figure 8c is relatively large compared to that of the other $1/v$ law isotope ^{59}Co , since a prominent neutron resonance exists at 4.91 eV. The deviation of s_4^H from s_2^W increases from 0% to 10% as the neutron temperature increases from 0 K to 1600 K. This deviation observed in the case of s_4^H is prominent compared to the case of s_4^W . The deviation in the case of s_4^W is only about 0.6% at a neutron temperature of 300 K. Considering the large size of the s -factor of ^{197}Au , a bias induced by a joining function ambiguity exceeds 1% . Since the s -factor of ^{197}Au is sometimes used as the standard nuclear value to determine other isotopes s -factor or resonance integrals, the bias of about 1% cannot be neglected. It should be noted that the bias increases furthermore as neutron temperature increases.

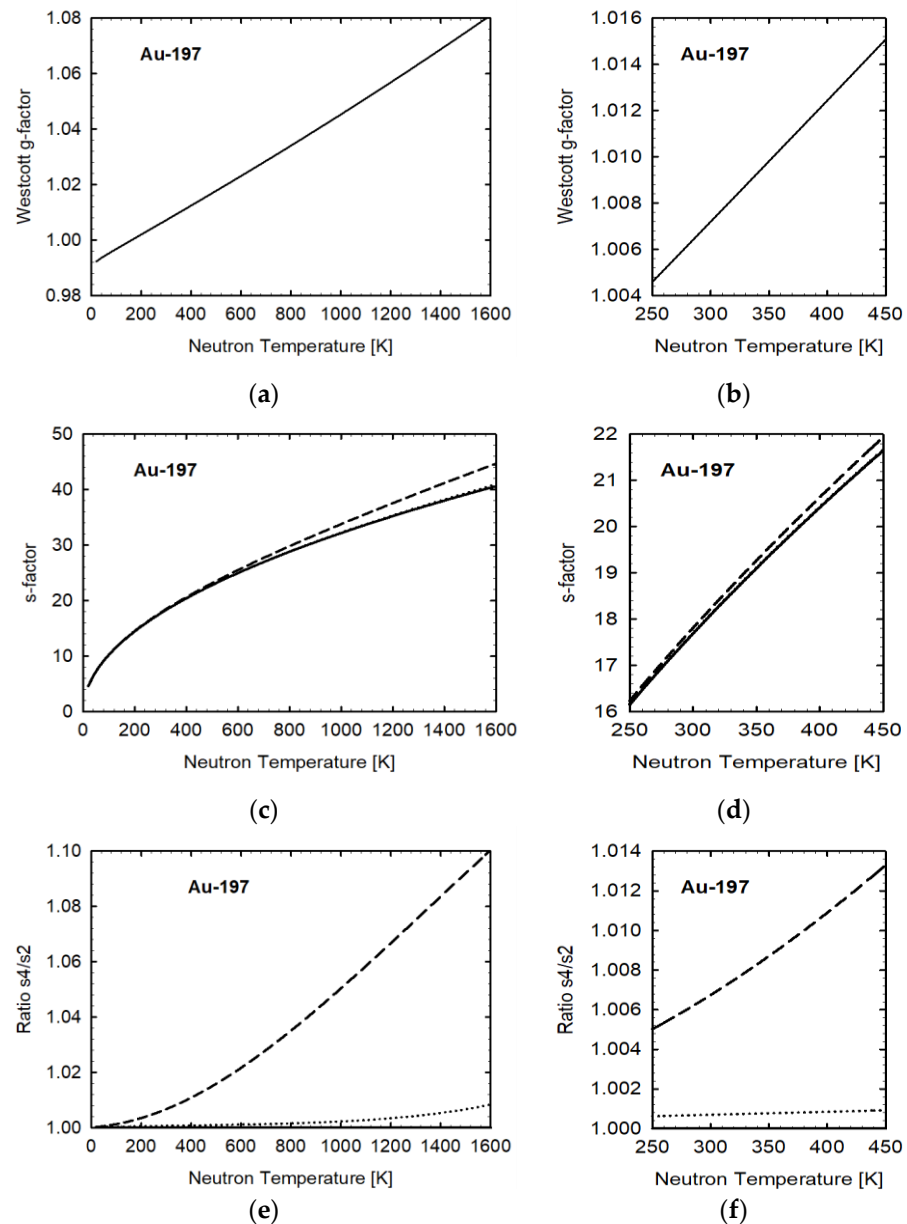


Figure 8. (a) Westcott g-factor for ^{197}Au as a function of neutron temperature T_n ; (b) Expanded figure of (a); (c) s-factors, s_2^W (solid line), s_4^W (dotted line), s_4^H (dashed line) for ^{197}Au as a function of neutron temperature T_n ; (d) Expanded figure of (c); (e) Ratios of s-factor s_4^W/s_2^W (dotted line) and s_4^H/s_2^W (dashed line) for ^{197}Au ; (f) Expanded figure of (e).

Figure 9a–f show results for ^{59}Co . The capture cross section of ^{59}Co is also used as the standard for thermal neutron capture cross sections and resonance integrals. The capture cross section of ^{59}Co obeys the $1/v$ law well, as shown in Figure 3b. Since there is no resonance below 10 eV, the deviation of the g-factor from the unity is extremely small, as shown in Figure 9a,b. The s-factors shown in Figure 9c,d for three joining functions are almost degenerating. As shown in Figure 9e,f, the deviation originating in a joining function ambiguity is less than 0.1% for a wide neutron temperature range. From the results for ^{59}Co , it is expected that the bias effect originating in a joining function shape is negligible for isotopes obeying the $1/v$ law well. The order of the bias for isotopes obeying the $1/v$ law would be roughly estimated from the results of ^{197}Au and ^{59}Co .

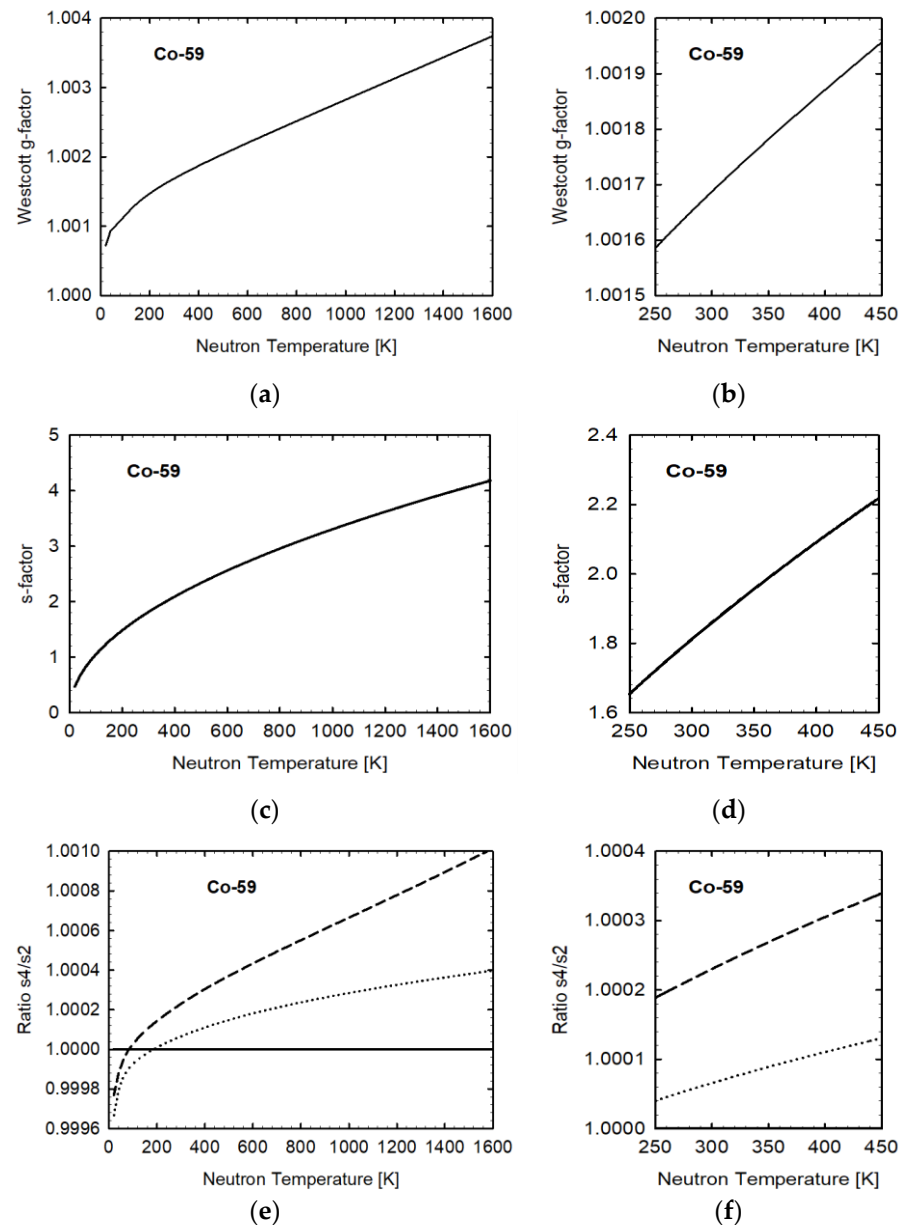


Figure 9. (a) Westcott g-factor for ^{59}Co as a function of neutron temperature T_n ; (b) Expanded figure of (a); (c) s-factors, s_2^W (solid line), s_4^W (dotted line), s_4^H (dashed line) for ^{59}Co as a function of neutron temperature T_n ; (d) Expanded figure of (c); (e) Ratios of s-factors, s_4^W/s_2^W (dotted line) and s_4^H/s_2^W (dashed line) for ^{59}Co ; (f) Expanded figure of (e).

Figure 10a–f show the results for ^{103}Rh . There is a huge resonance at 1.26 eV in ^{103}Rh . Therefore, the g-factor increases as neutron temperature increases, as shown in Figure 10a,b. The s-factor also monotonically increases as a function of neutron temperature, as for ^{197}Au . However, the differences among s_2^W , s_4^W , and s_4^H are more notable compared to those for ^{197}Au , as shown in Figure 10c,d. The deviation of s_4^W and s_4^H from s_2^W increases from 0% to about 30% as neutron temperature increases from 0 K to 1600 K. A prominent deviation is observed in the case of s_4^W for a neutron temperature less than about 1100 K. The deviation is about 7% at a neutron temperature of 300 K. Considering the large size of the s-factor of ^{103}Rh , a bias induced by a joining function ambiguity exceeds 3%, even in the case of epithermal neutron index $r = 0.1$.

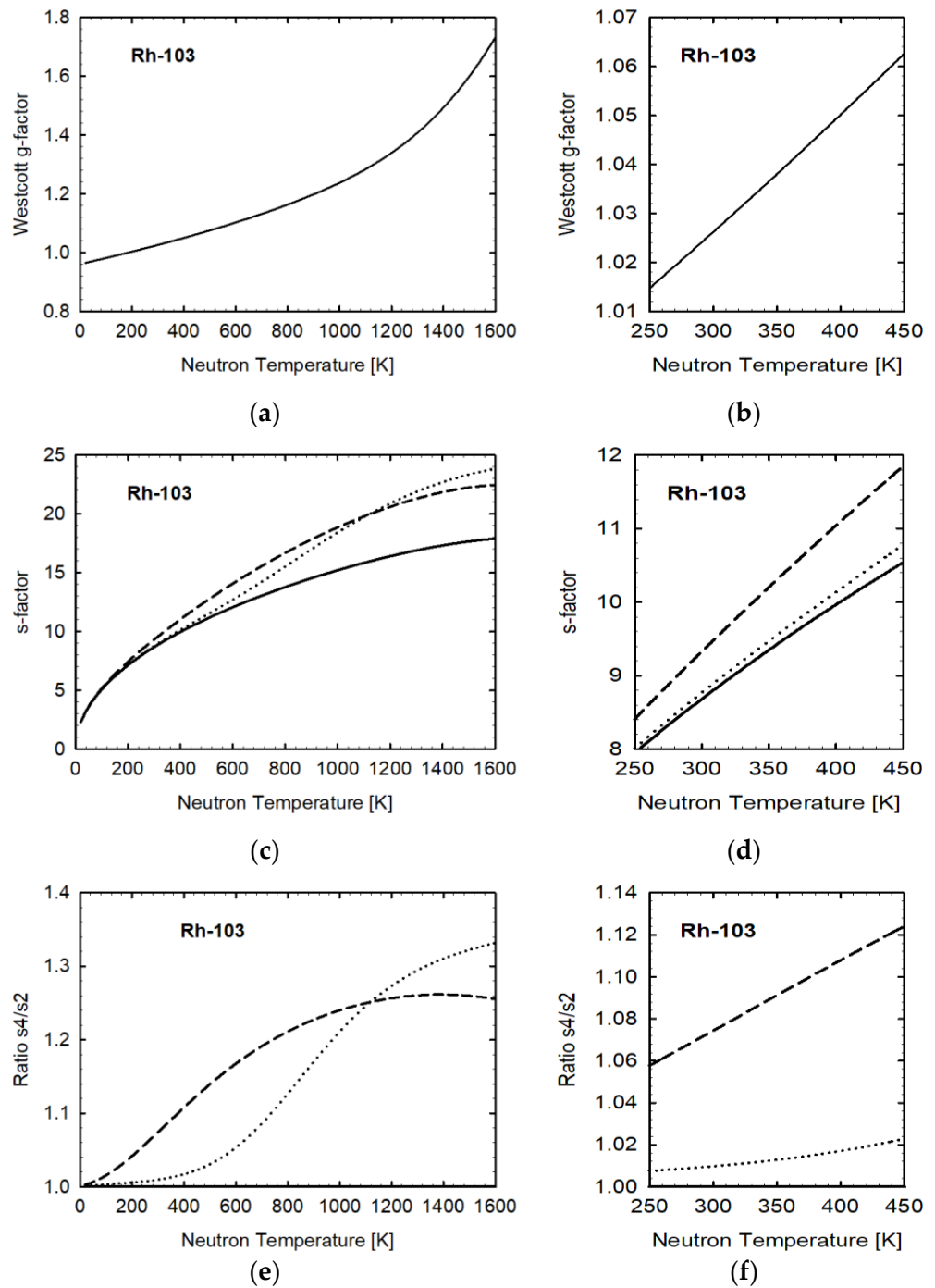


Figure 10. (a) Westcott g -factor for ^{103}Rh as a function of neutron temperature T_n ; (b) Expanded figure of (a); (c) s -factors, s_2^W (solid line), s_4^W (dotted line), s_4^H (dashed line) for ^{103}Rh as a function of neutron temperature T_n ; (d) Expanded figure of (c); (e) Ratios of s -factors, s_4^W/s_2^W (dotted line) and s_4^H/s_2^W (dashed line) for ^{103}Rh ; (f) Expanded figure of (e).

Figure 11a–f shows the results for ^{115}In . There is a huge resonance at 1.46 eV in ^{115}In . The neutron temperature dependence of the g - and s -factor is close to that observed for ^{103}Rh . At the neutron temperature of 300 K, the bias induced by a joining function ambiguity reaches also about 3% in the case of epithermal neutron index $r = 0.1$.

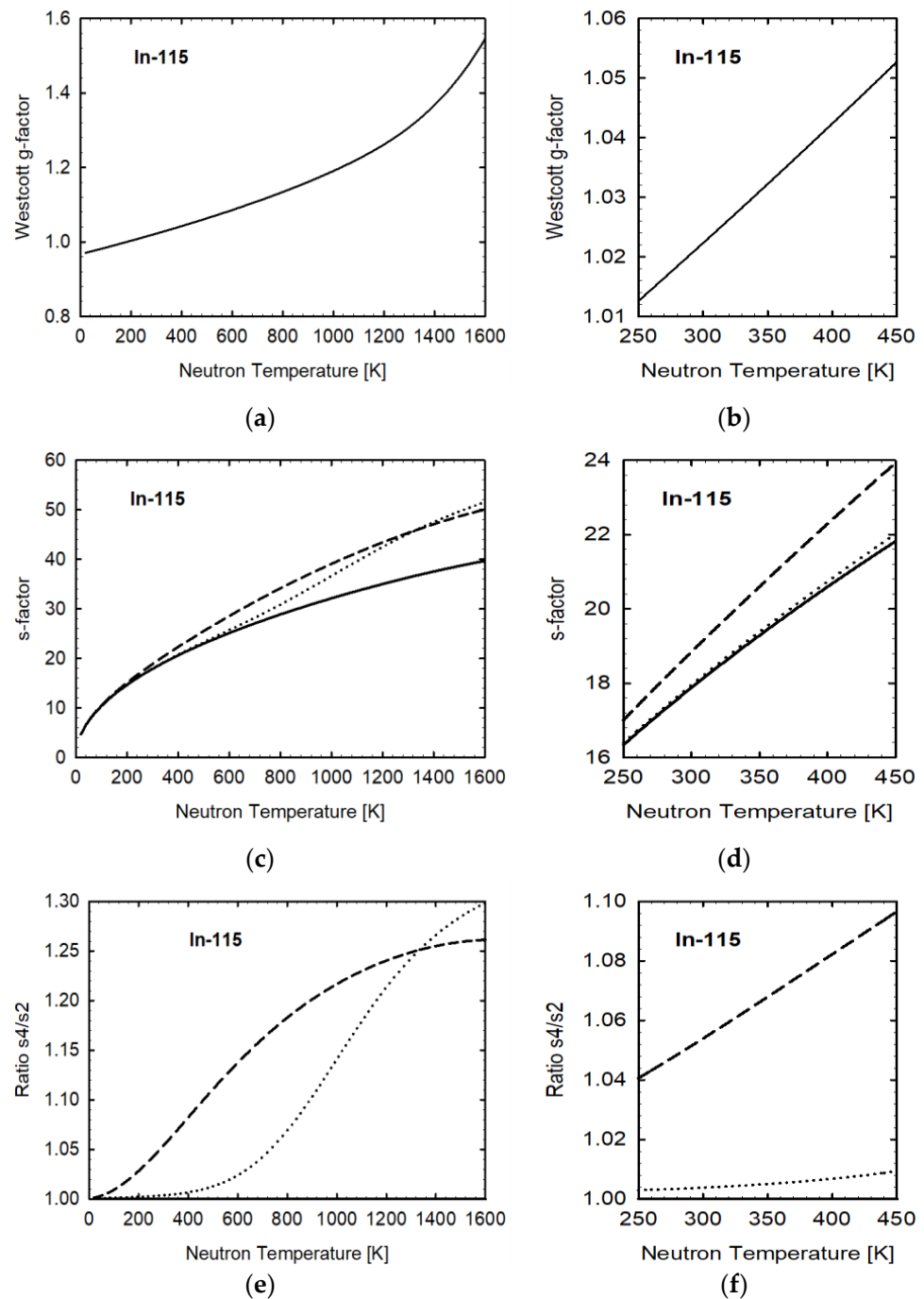


Figure 11. (a) Westcott g -factor for ^{115}In as a function of neutron temperature T_n ; (b) Expanded figure of (a); (c) s -factors, s_2^W (solid line), s_4^W (dotted line), s_4^H (dashed line) for ^{115}In as a function of neutron temperature T_n ; (d) Expanded figure of (c); (e) Ratios of s -factors, s_4^W/s_2^W (dotted line) and s_4^H/s_2^W (dashed line) for ^{115}In ; (f) Expanded figure of (e).

Figure 12a–f shows the results for ^{177}Hf . There are huge resonances at 1.10 eV and 2.39 eV in ^{177}Hf . The neutron temperature dependence of the g - and s -factors is similar to those for ^{103}Rh and ^{115}In . At the neutron temperature of 300 K, the bias induced by a joining function ambiguity exceeds 3% as for ^{103}Rh and ^{115}In .

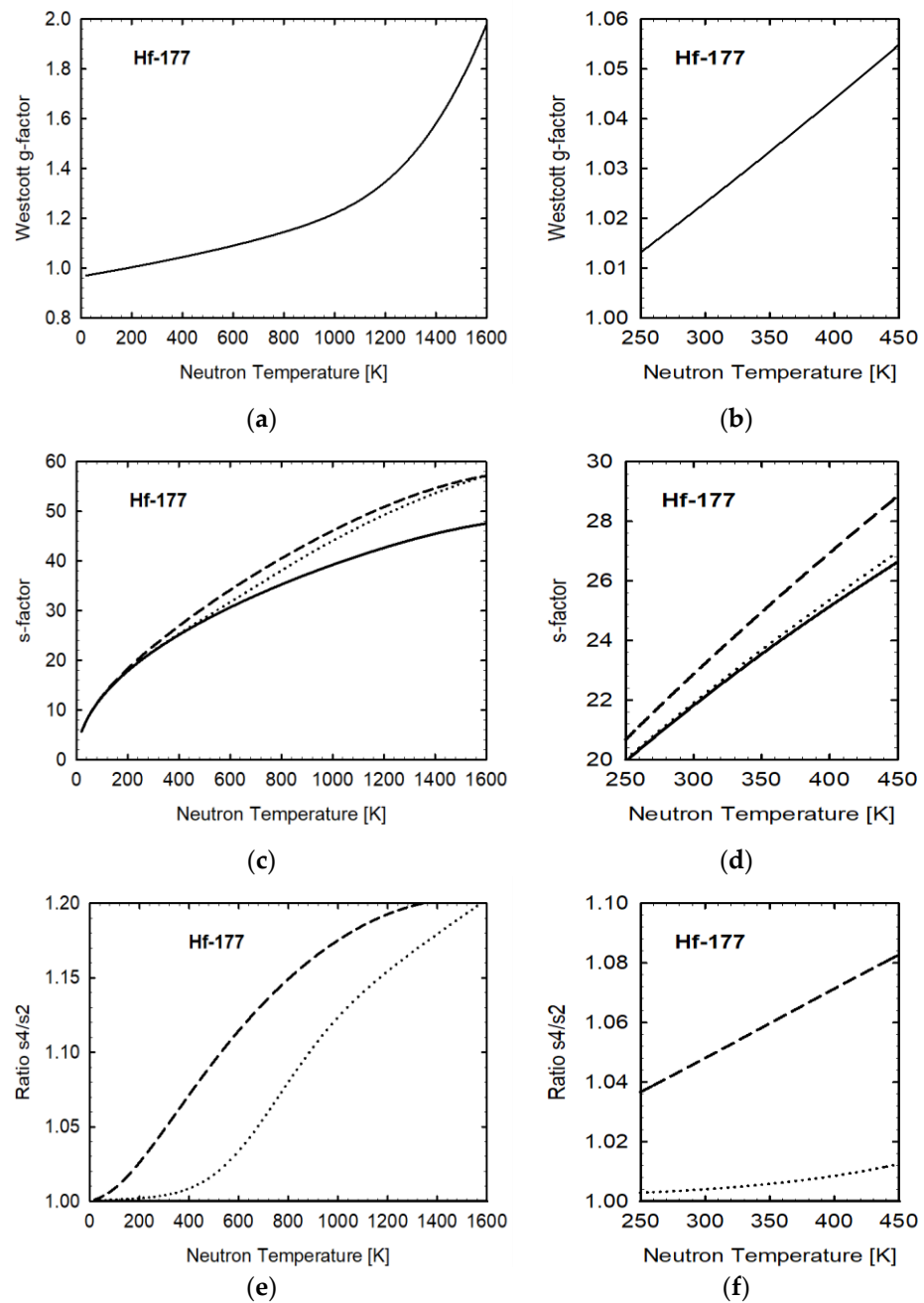


Figure 12. (a) Westcott g -factor for ^{177}Hf as a function of neutron temperature T_n ; (b) Expanded figure of (a); (c) s -factors, s_2^W (solid line), s_4^W (dotted line), s_4^H (dashed line) for ^{177}Hf as a function of neutron temperature T_n ; (d) Expanded figure of (c); (e) Ratios of s -factors, s_4^W/s_2^W (dotted line) and s_4^H/s_2^W (dashed line) for ^{177}Hf ; (f) Expanded figure of (e).

Figure 13a–f shows the results for ^{226}Ra . There is a huge resonance at 0.54 eV in ^{226}Ra . The neutron temperature dependence of the g -factor is similar to that for ^{241}Am , although the absolute value for ^{226}Ra increases more rapidly as neutron temperature increases. On the other hand, the neutron temperature dependence of the s -factor is similar to that for ^{151}Eu . The differences among s_2^W , s_4^W , and s_4^H are more notable compared to those for ^{103}Rh , ^{115}In , and ^{177}Hf at the neutron temperature of 300 K, as shown in Figure 13e,f. Therefore, a huge bias effect originating in a joining function ambiguity is expected at the neutron temperature at 300 K.

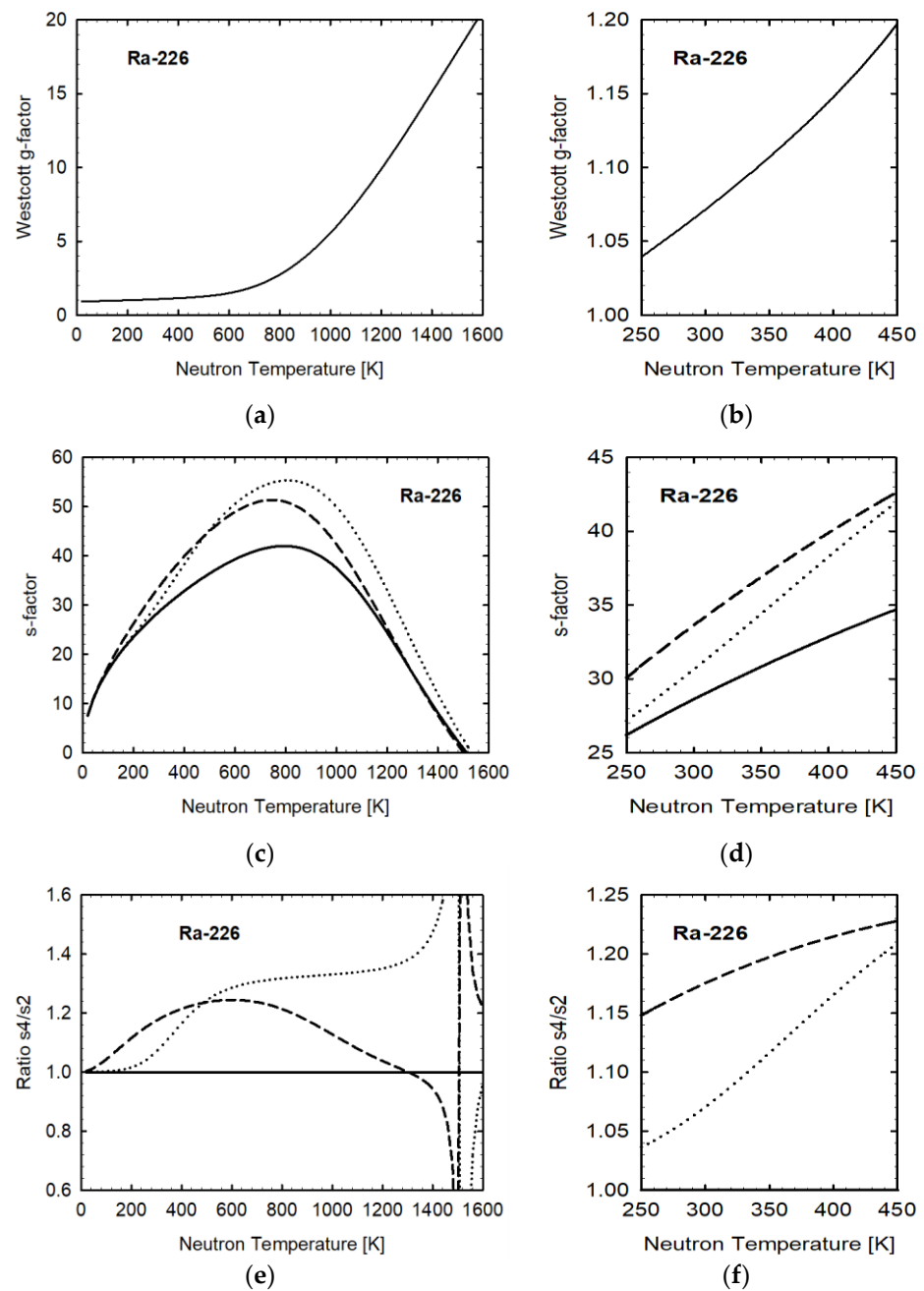
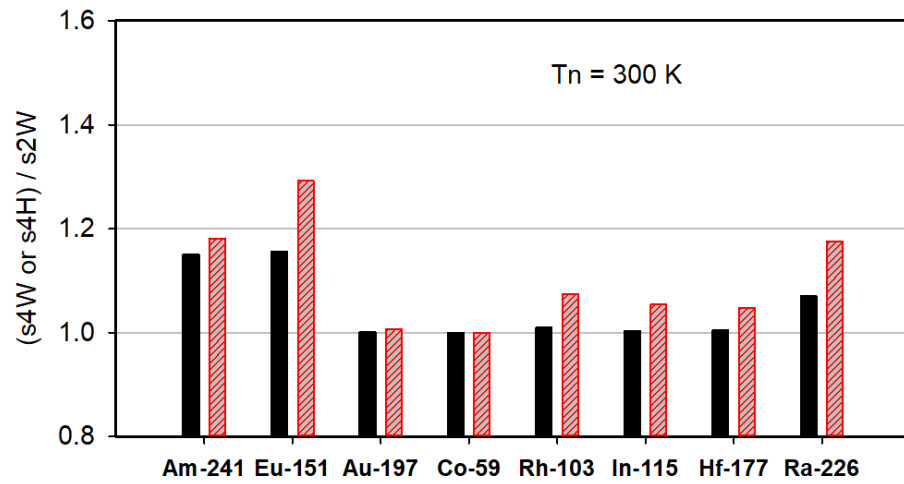


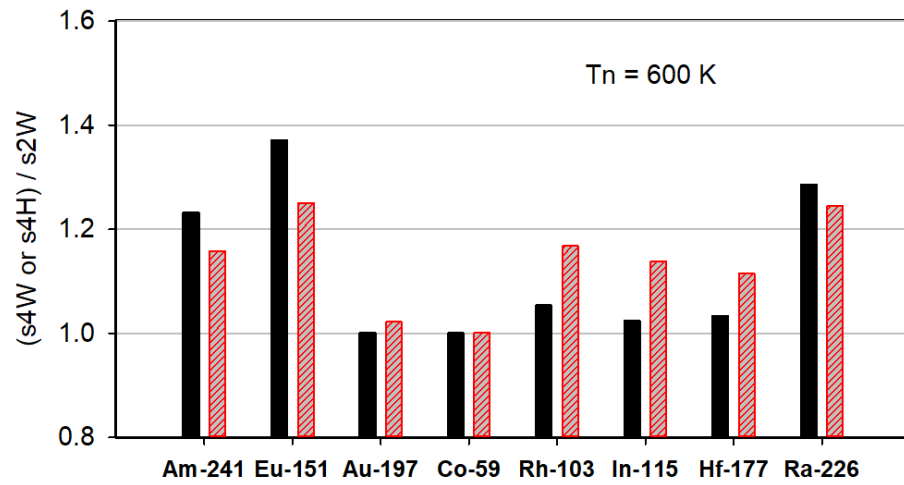
Figure 13. (a) Westcott g -factor for ^{226}Ra as a function of neutron temperature T_n ; (b) Expanded figure of (a); (c) s -factors, s_2^W (solid line), s_4^W (dotted line), s_4^H (dashed line) for ^{226}Ra as a function of neutron temperature T_n ; (d) Expanded figure of (c); (e) Ratios of s -factors, s_4^W/s_2^W (dotted line) and s_4^H/s_2^W (dashed line) for ^{226}Ra ; (f) Expanded figure of (e).

3.4. Bias on the s -Factor by the Joining Function

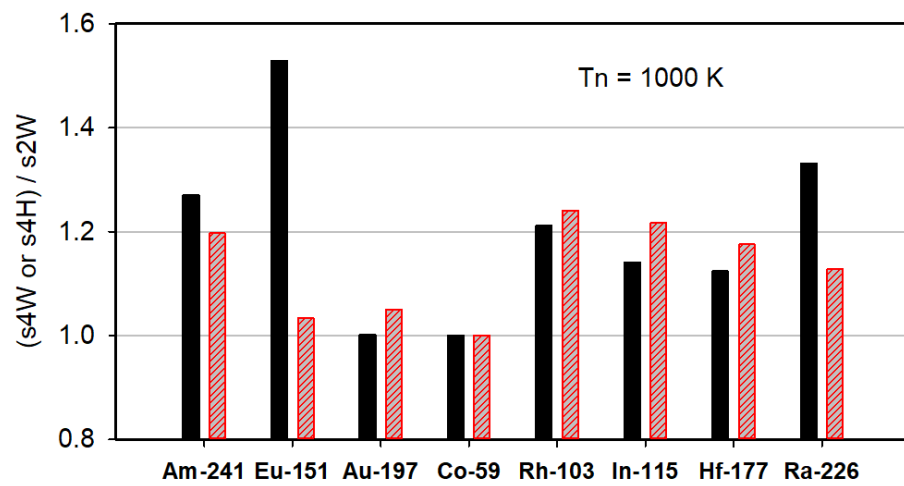
Biases on s -factor originating in a joining function are compared among ^{241}Am , ^{151}Eu , ^{197}Au , ^{59}Co , ^{103}Rh , ^{115}In , ^{177}Hf , and ^{226}Ra in Figure 14. The ratios s_4^W/s_2^W and s_4^H/s_2^W are shown by black bars and red-hatched bars. The results for neutron temperature of 300 K, 600 K, and 1000 K are shown in Figure 14a–c, respectively.



(a)



(b)



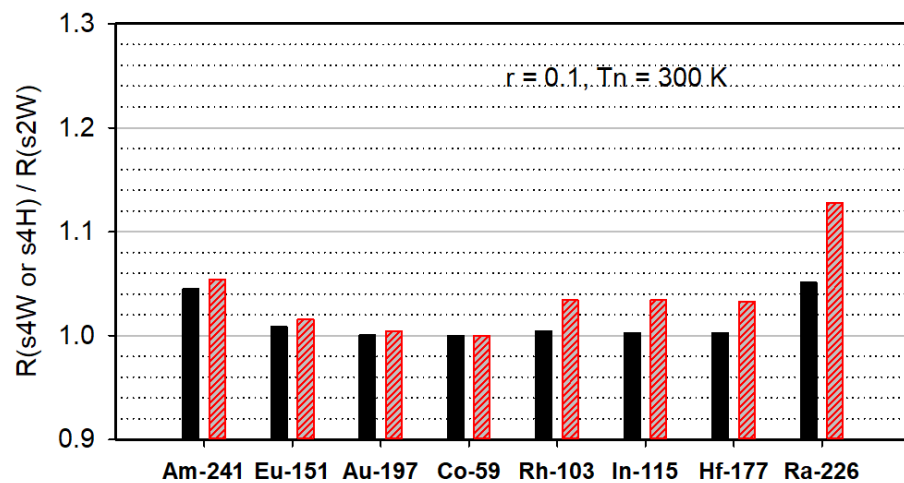
(c)

Figure 14. (a) Ratios of s-factors, s_4^W / s_2^W (black bar), and s_4^H / s_2^W (red dashed bar) for ^{241}Am , ^{151}Eu , ^{197}Au , ^{59}Co , ^{103}Rh , ^{115}In , ^{177}Hf , and ^{226}Ra at the neutron temperature of 300 K; (b) Same as (a) at the neutron temperature of 600 K; (c) Same as (a) at the neutron temperature of 1000 K.

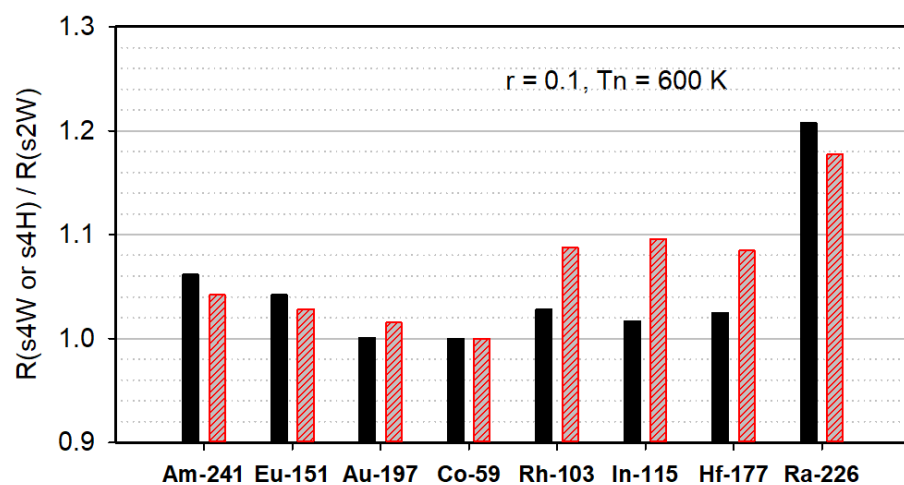
As shown in Figure 14a, large biases exceeding 10% occur in the cases of ^{241}Am , ^{151}Eu , and ^{226}Ra at the neutron temperature of 300 K. The largest deviation from the unity is observed in the case of ^{151}Eu for s_4^H/s_2^W , corresponding to about 29%. In the case of the neutron temperature of 600 K, the largest deviation from the unity is also observed for ^{151}Eu , though for s_4^W/s_2^W , corresponding to about 37%. In the case of the neutron temperature of 1000 K, the largest deviation from the unity is again observed for ^{151}Eu , for s_4^W/s_2^W , exceeding 50%.

3.5. Bias on the Reaction Rate by the Joining Function

In order to estimate the bias on the reaction rate originating in a joining function, Equation (1) is used. The size of the bias on the reaction rate depends on the value of the epithermal index r . Figure 15 shows biases on the reaction rate originating in a joining function in the case of $r = 0.1$; the value of r depends on the irradiation facility and irradiation position and ranges typically from 0 to 0.2. The ratios $R(s_4^W)/R(s_2^W)$ and $R(s_4^H)/R(s_2^W)$ are shown by black bars and red-hatched bars. The results in the cases of neutron temperatures of 300 K, 600 K, and 1000 K are shown in Figure 15a–c, respectively.



(a)



(b)

Figure 15. Cont.

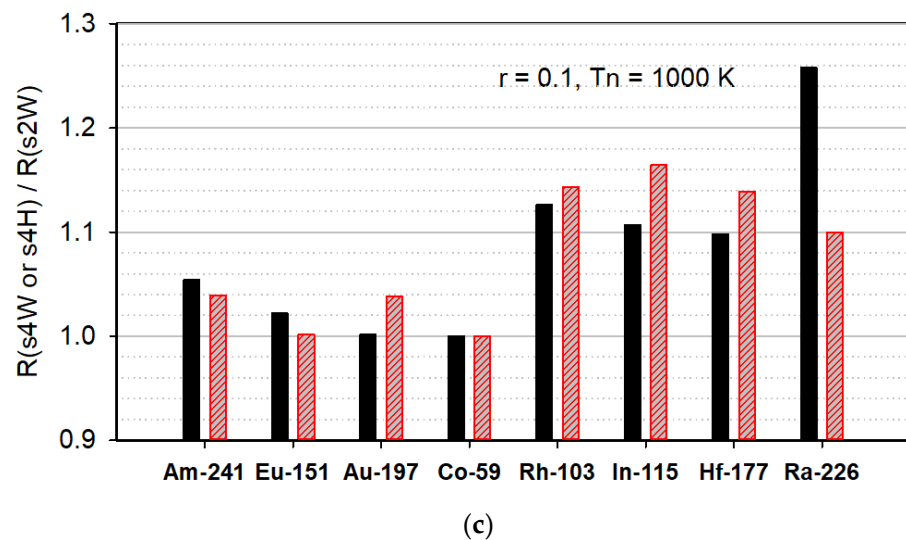


Figure 15. (a) Ratios of reaction rates in the case of $r = 0.1$, $R(s_4^W) / R(s_2^W)$ (black bar) and $R(s_4^H) / R(s_2^W)$ (red dashed bar) for ^{241}Am , ^{151}Eu , ^{197}Au , ^{59}Co , ^{103}Rh , ^{115}In , ^{177}Hf , and ^{226}Ra at the neutron temperature of 300 K; (b) Same as (a) at the neutron temperature of 600 K; (c) Same as (a) at the neutron temperature of 1000 K.

As shown in Figure 15a, large biases exceeding 10% occur only in the cases of ^{226}Ra at the neutron temperature of 300 K, for $R(s_4^H) / R(s_2^W)$. At the neutron temperature of 600 K, the largest deviation from the unity is also observed in ^{226}Ra , but for $R(s_4^W) / R(s_2^W)$, that exceeds 20%. In the case of the neutron temperature of 1000 K, the largest deviation from the unity is again observed in ^{226}Ra for s_4^W / s_2^W and it is about 26%.

The reason that the largest bias is not observed in ^{151}Eu but in ^{226}Ra is explained as follows: for the reaction rate, the bias is moderate due to the opposite effect exerted by the g-factor and s-factor on the reaction rate. This is demonstrated for ^{151}Eu , by comparing Figures 5a and 7a.

The height of a bump in a joining function at its peak position is about 26–31%, as shown in Figure 1. The peak position of the bump increases as neutron temperature increases. When an energy of a first huge resonance is close to the peak position, a large bias is anticipated in the s-factor.

In this work, a bias originating in neutron nuclear data is not considered. It should be noted here that there is sometimes an uncertainty in the order of 10% even in well-investigated neutron nuclear data, as demonstrated in recent works on ^{241}Am [10,17,18].

4. Conclusions

Bias effects have been investigated on the g- and s-factors in the Westcott convention. As origins of biases, a joining function shape, neutron temperature, and sample temperature, have been investigated. The quantitative results are given for 8 isotopes, i.e., ^{241}Am , ^{151}Eu , ^{197}Au , ^{59}Co , ^{103}Rh , ^{115}In , ^{177}Hf , and ^{226}Ra . The results show the bias induced by sample temperature is small, in the order of 0.1% for the g-factor and in the order of 1% for the s-factor. Biases induced by a joining function shape for the s-factor are shown to be in the order of 10% for many non-1/v isotopes. The bias size for the reaction rate in the case of an epithermal neutron index $r = 0.1$ is also shown. The largest bias is obtained for ^{226}Ra among the eight isotopes. The order of bias size for the s-factor or reaction rate can be grasped from the results given for the eight isotopes in the figures. For non-1/v isotopes, the bias effect originating in a joining function shape needs to be carefully investigated. The formulas to calculate g- and s-factors in this paper enable bias calculation without a special code. If the size of the calculated bias is close to the required accuracy of NAA, a more careful study on neutron energy spectrum at the irradiation position and energy-dependent nuclear data is recommended.

Funding: This research received no external funding.

Data Availability Statement: Not applicable.

Conflicts of Interest: The authors declare no conflict of interest.

References

1. Westcott, C.H.; Walker, W.H.; Alexander, T.K. *Effective Cross Sections and Cadmium Ratios for the Neutron Spectra of Thermal Reactors*; A/CONF.15/P/202; AECL-612 202 1–16; U.S. Department of Energy, Office of Scientific and Technical Information: Oak Ridge, TN, USA, 1959. Available online: <https://osti.gov/servlets/purl/4279663> (accessed on 15 July 2021).
2. Harada, H.; Sekine, T.; Hatsukawa, Y.; Shigeta, N.; Kobayashi, K.; Ohtsuki, T.; Katoh, T. Measurement of the Thermal Neutron Cross Section of the $^{90}\text{Sr}(n,\gamma)^{91}\text{Sr}$ Reaction. *J. Nucl. Sci. Technol.* **1994**, *31*, 173–179. [[CrossRef](#)]
3. Harada, H.; Nakamura, S.; Katoh, T.; Ogata, Y. Measurement of Thermal Neutron Cross Section and Resonance Integral of the Reaction $^{99}\text{Tc}(n,\gamma)^{100}\text{Tc}$. *J. Nucl. Sci. Technol.* **1995**, *32*, 395–403. [[CrossRef](#)]
4. Ohta, M.; Nakamura, S.; Harada, H.; Fujii, T.; Yamana, H. Measurement of Effective Capture Cross Section of Americium-243 for Thermal Neutrons. *J. Nucl. Sci. Technol.* **2006**, *43*, 1441–1445. [[CrossRef](#)]
5. Nakamura, S.; Ohta, M.; Harada, H.; Fujii, T.; Yamana, H. Thermal-Neutron Capture Cross Section and Resonance Integral of Americium-241. *J. Nucl. Sci. Technol.* **2007**, *44*, 1500–1508. [[CrossRef](#)]
6. Ryves, T.B. A new thermal neutron flux convention. *Metrologia* **1969**, *3*, 205–215. [[CrossRef](#)]
7. Harada, H.; Takayama, N.; Komeda, M. A new convention for the epithermal neutron spectrum for improving accuracy of resonance integrals. *J. Phys. Commun.* **2020**, *4*, 085004. [[CrossRef](#)]
8. Trkov, A.; Radulović, V. Nuclear reactions and physical models for neutron activation analysis. *J. Rad. Nucl. Chem.* **2015**, *304*, 763–778. [[CrossRef](#)]
9. Westcott, C.H. *Effective Cross Section Values for Well-Moderated Thermal Reactor Spectra*, 3rd ed.; CRRP-960; Atomic Energy of Canada Ltd.: Chalk River, ON, Canada, 1970; pp. 1–37.
10. Žerovnik, G.; Schillebeeckx, P.; Becker, B.; Fiorito, L.; Harada, H.; Kopecky, S.; Radulović, V.; Sano, T. Systematic effects on cross section data derived from reaction rates in reactor spectra and a re-analysis of ^{241}Am reactor activation measurements. *Nucl. Inst. Method* **2018**, *A877*, 300–313. [[CrossRef](#)]
11. Van Sluijs, R. The Westcott convention converted in the extended version of the modified Hogdahl convention. *J. Rad. Nucl. Chem.* **2019**, *319*, 1277–1282. [[CrossRef](#)]
12. De Corte, F.; De Wispelaere, A. The use of a Zr–Au–Lu alloy for calibrating the irradiation facility in k_0 -NAA and for general neutron spectrum monitoring. *J. Rad. Nucl. Chem.* **2005**, *263*, 653–657. [[CrossRef](#)]
13. Shcherbakov, O.; Harada, H. Resonance Self-Shielding Corrections for Activation Cross Section Measurements. *J. Nucl. Sci. Technol.* **2002**, *39*, 548–553. [[CrossRef](#)]
14. ENDF Graph. Available online: https://wwwndc.jaea.go.jp/ENDF_Graph/ (accessed on 28 May 2021).
15. Shibata, K.; Iwamoto, O.; Nakagawa, T.; Iwamoto, N.; Ichihara, A.; Kunieda, S.; Chiba, S.; Furutaka, K.; Otuka, N.; Ohsawa, T.; et al. JENDL-4.0: A new library for nuclear science and engineering. *J. Nucl. Sci. Technol.* **2011**, *48*, 1–30. [[CrossRef](#)]
16. Fröhner, F.H. *Applied Neutron Resonance Theory*; Reprinted from Nuclear Theory for Applications, p. 59 ff.; International Centre for Theoretical Physics: Trieste, Italy, 1980.
17. OECD/NEA/WPEC/SG-41 Report in Nuclear Science. Improving Nuclear Data Accuracy of ^{241}Am Capture cross Section. 2020. NEA/NSC/R(2020)2 1–45. Available online: [https://www.oecd.org/officialdocuments/publicdisplaydocumentpdf/?cote=NEA/NSC/R\(2020\)2&docLanguage=En](https://www.oecd.org/officialdocuments/publicdisplaydocumentpdf/?cote=NEA/NSC/R(2020)2&docLanguage=En) (accessed on 15 July 2021).
18. Terada, K.; Kimura, A.; Nakao, T.; Nakamura, S.; Mizuyama, K.; Iwamoto, N.; Iwamoto, O.; Harada, H.; Katabuchi, T.; Igashira, M.; et al. Measurements of neutron total and capture cross sections of ^{241}Am with ANNRI at J-PARC. *J. Nucl. Sci. Technol.* **2018**, *55*, 1198–1211. [[CrossRef](#)]